Hierarchical porosity in additively manufactured bioengineering scaffolds: fabrication & characterisation

Faezeh Shalchy[a,*], Christopher Lovell[b], Atul Bhaskar[a]

[a] *Faculty of Engineering and Physical Sciences, University of Southampton, Southampton UK*

[b] *Lucideon Ltd, Stoke-on-Trent, UK*

Abstract

Biomedical scaffolds with a high degree of porosity are known to facilitate the growth of healthy functioning tissues. In this study, scaffolds with hierarchical porosity are manufactured and their mechanical and thermal properties are characterised. Multi-scale porosity is achieved in scaffolds fabricated by fused deposition modelling in a novel way. Random intrinsic porosity at micron length scale obtained from particulate leaching is combined with the structured extrinsic porosity at millimeter length scales afforded by controlling the spacing between filaments. Polylactic acid (PLA) is blended with Polyvinyl alcohol (PVA) and an inorganic sacrificial phase, sodium chloride (NaCl), to produce pores at length scales of up to two orders of magnitude smaller than the inter-filament voids within 3D printed lattices. The specific elastic modulus and specific strength are maximised by optimising the polymer blends. The porosity level and pore size distribution of the foamy filaments within lattices are quantified statistically. Compression tests are

*Corresponding author

Email address: f.shalchy@soton.ac.uk (Faezeh Shalchy)

performed on the porous samples and their mechanical response is attributed to their microstructure and density using cellular solid models that possess power law dependence associated with various elastic deformation mechanisms of cell walls. The relationship between pore architecture, pore connectivity, the blend material composition, and mechanical response of produced foams is brought out. Foams obtained using the PLA:PVA:NaCl 42%-18%-40% material blends show relatively high specific elastic modulus, specific strength and strain at failure. A quadratic power law relating the Young's modulus with the relative density is experimentally obtained, which is consistent with theoretical models for open-cell foams. 3D printing with blends, followed by leaching, produces structures with cumulative intrinsic and extrinsic porosity as high as 80%, in addition to good mechanical integrity.
Keywords:
Hierarchical porosity, 3D printing, Biomedical scaffold, Particulate leaching, Cellular solid models, Open-cell foams

---

1. Introduction and Background

Organ and tissue transplant is of great current interest, as they are promising interventions to improve the quality of life and to increase life expectancy. A recent report by Organ Procurement and Transplantation Network (OPTN) registered over a hundred thousand patients in the USA awaiting transplant at the end of June, 2018, while 14,780 transplants were performed in 2018 [1]. Regenerative medicine in general and Tissue engineering (TE) in particular is a field that aim to overcome this problem. TE scaffolds are engineered structures that provide desirable mechanical support and cellular environment to enable cell regeneration, and subsequently organ formation [2; 3; 4]. A biomedical scaffold needs to provide the necessary structural support for newly generated tissue, and must possess suitable chemical and physical properties to promote cell/substrate interaction, in order to allow cell attachment and migration. Moreover, it should posses high porosity to facilitate cell in-growth, and be mechanically compatible to the native physical condition of the tissue [5]. The goal of this study is to tailor hierarchical microstructure in TE scaffolds by combining 3D printing and a conventional manufacturing method.

In order to effectively deliver nutrients to cells to regenerate on scaffolds, porosity is essential [6]. The precise effect of porosity on cell behaviour depends on the cell type and pore size [7; 8; 9]. Hence, the optimum scaffold porosity needs to be determined based on the TE application and the desired cell function. For instance, in bone tissue regeneration, 35% to 80% porosity and the pore size around 10 μm to 200 μm have been reported to improve cell regeneration [8; 9]. The degree of interconnectivity is mostly determined

qualitatively [10; 11]; however, in the recent years, approaches have been proposed to quantify this parameter [12; 13]. These studies usually involve the use of image analysis, in conjunction with algorithms involving computational geometry aimed at automating the spatial information to determine the pore interconnectivity [14]. There have been many manufacturing methods proposed for TE applications, and various techniques have been developed to fabricate porous structures from synthetic and natural materials such as polymers and bioceramics. The main focus in these methods is to create scaffolds having a continuous, interconnected pore structure and pore size according to the intended application. On the other hand, increasing pore interconnectivity and porosity level, adversely affect mechanical properties of the scaffolds. One of the goals of our study is to optimise this porosity level as well as pore size and shape to achieve high specific strength and elastic modulus.

Phase separation [15; 16], melt moulding [17; 18], freeze-drying [19; 20; 21; 22] and solution casting [23] are among the conventional scaffold fabrication methods reported in the literature. A drawback of these methods, is their incapability of producing structures with precisely controlled pores size, geometry, and interconnectivity. For instance, solvent-casting technique cannot guarantee interconnected pores [24]. Moreover, the residual organic solvent increases the risk of toxicity and carcinogenicity, if one were to use the fabricated structures for medical applications by methods such as solvent casting, phase separation, and gas foaming. These processes typically involve the use of chloroform and methylene chloride, to dissolve synthetic polymers at some stage. These are in addition to the difficulty that pore size

in random foams is usually associated with process parameters of manufacturing in a statistical way. By contrast, pores could be very regular, with variations up to manufacturing tolerances for lattices, if one uses a computer controlled process such as additive manufacturing (AM). This method is capable of fabricating scaffolds with interconnected porosity, while providing *precisely controlled internal architecture and porosity.* However, the pore size achievable by the use of spaced array of fused stream of molten matter (also known as "beads"; we will refer to them as filaments within a lattice) is quite large compared to that required for enhancing bio-tribological benefits in the cellular response of biomedical scaffolds. Yet, such a pore size of the order of a fraction of a millimeter (but much larger than tens of microns) is useful in biomedical scaffolds for enabling nutrient transport through voids and cell growth into empty spaces. A solution to the demand of two-level porosity is to fabricate structures with hierarchical porosity —pores and surface features at small length scales for facilitating cell attachment, while providing larger pores for in-growth of the tissue. The present work is motivated by this interesting possibility.

AM is an efficient route to fabricate scaffolds with complex microstructure and interconnected porosity of specified shape and size [25; 26; 27]. Moreover, increasingly wider range of materials compatible with AM makes it promising for many diverse applications such as biomedical scaffolds [28; 29; 30]. Hence, there is an increasing use of additive manufacturing and, therefore, the need to improve the understanding all aspects of the fabricated products is more than ever before. There is a great current interest to address the challenge of introducing porosity at multiple length scales. Recent stud-

ies, using AM techniques, have had some success with the fabrication of porous scaffolds. Mu et al. (2017) [31] fabricated porous structures by mixing Sodium Chloride (NaCl or common salt) with photo-curable resin; after which, salt was dissolved. They used Digital Light Processing (DLP) to fabricate porous scaffolds. However, not many bio-compatible polymers are photo-curable, which poses a serious limitation to materials available for scaffold fabrication. Jakus et al. (2018) [32] synthesized an ink by adding $CuSO_4$ in to polylactide-co-glycolide (PLGA) for inkjet 3D printing. Scaffolds with 66.6% to 94.4% porosity resulting in material with 112.6 MPa to 2.7 MPa elastic moduli were fabricated. They show that this process can be extended to other materials including graphene, metals, and ceramics [32]. Bone tissue engineering benefits from properties of bioceramics and bioactive glasses. Baino et al. presented a review on bioceramics and bioactive glasses, their features and suitable manufacturing methods including 3D printing [33].

The aim of this study is to design, fabricate and characterise hierarchically structured scaffolds with tailored macro/micro-porosity architectures, such as those frequently used for bone tissue engineering applications. Porosity at finer scales is achievable by AM process of material mixtures and blends, followed by leaching out a sacrificial phase from the material. These structures contain both extrinsic [1] and intrinsic porosity [2]. Multi-scale porosity using

[1] Porosity which is inherent to the structure/arrangement, not the material. This porosity can be controlled through design of the structure.

[2] Porosity at mesoscopic length scales which is inherent to the material from which the structure is formed. This type of porosity is mostly random and does not possess any long-range order.

fused deposition modelling (FDM) process, which is the most economical and commonly used AM process, as proposed here, is expected to significantly increase the overall porosity of TE scaffolds while they retain their mechanical integrity. We believe that combining intrinsic porosity and extrinsic porosity throughout the whole volume of scaffolds would be beneficial for cell regeneration. Herein, we manufacture and characterise ultra-porous TE scaffolds intended to promote cell regeneration in scaffolds fabricated by AM. Porous 3D printed lattice structures are being currently used for many biomedical applications. The idea of using a sacrificial phase to create porosity in material has been there for a while [34; 35]. However, their combined use within FDM 3D printed structures, and with multiple sacrificial phases as reported here, to create a hierarchical porosity appears to be novel. Inorganic as well as polymeric sacrificial phases are employed to introduce intrinsic porosity to the 3D printed lattice structure —the extrinsic porosity is controlled by the computer code that dictates the spacing of micro-filaments. This method of achieving multi-scale porosity can be easily applied to other biomaterials such as bioceramics. Since the mechanical integrity of biomedical scaffolds is important in their medical success, mechanical testing and cellular solid theoretical approach [36; 37] are employed to investigate their mechanical response.

2. Materials and Methods

2.1. Base Materials:

Polylactic acid (PLA) is a polyester of lactide used in this study due to its compatibility to FDM 3D printing and frequent use in biomedical

applications[38]. Many researchers have studied their chemical to mechanical properties [39; 40; 41; 42; 43; 44]. Considering its desirable physical properties and biocompatibility, this material has been extensively used in many applications such as tissue engineering scaffolds [45], dental materials, ophthalmic implants, fracture fixation [46; 47], and drug delivery systems [48; 49; 50]. PLA (PURASORB PL 38 (Poly(L-lactide)) used in our study was procured from Corbion, Amsterdam The Netherlands. High molecular weight PLA was chosen due to its high viscosity and subsequently better printability.

Polyvinyl alcohol (PVA) and NaCl are used as porogen [3] in this study. PVA (MOWIFLEX^{TM} C 17) was acquired from Kuraray Europe GmbH, Hattersheim, Germany. This material can be used as water soluble support material in FDM 3D printing. Therefore, it is compatible with the FDM 3D printing parameters such as the normal printing temperature range. Common salt was another phase chosen to act as a porogen. The advantage of using this material is that it can be washed out at room temperature using water as solvent. The range of particle sizes of NaCl can help create a structure with uniform and interconnected porosity. The feasibility of using NaCl as a porogen in conjunction with FDM 3D printing is investigated here. Sodium chloride crystals were ground into smaller particles using ball-milling for five one-minute rounds then were separated into defined size ranges using brass sieves with 150 μm nominal sieve openings. Subsequently, the parti-

[3] A porogen is a pore generating component in a material blend. After being introduced into the blend, it is removed either by dissolving it in a solvent, or by processes such as release of a gaseous phase upon heating in order to produce voids such as those in foams.

Table 1: Mechanical and thermal properties of the materials used to prepare the blends

Material Properties	PLA [39]	PVA [51]	NaCl [52]
Young's Modulus (GPa)	3.5	2.4	39.9
Strength (MPa)	59	45	3.9
Glass Transition Temperature (°C)	60-65	60	-
Melting Temperature (°C)	170-200	170	801
Density (g/cm^3)	1.3	0.9-1.2	2.2

cle size distribution was measured using a Malvern Panalytical Master Sizer 3000. On the average, 90% of the particles were in the range of 74 μm. Mechanical and thermal properties of PLA, PVA and NaCl are presented in table 1.

2.2. Scaffold Fabrication

Three different types of blend compositions were prepared using three combinations of porogens: (1) PVA as porogen, (2) NaCl as porogen, and (3) a combination of PVA and NaCl, both used as porogens. Each blend leads to porous materials with different microstructures, mechanical and thermal properties. Selected weight fractions of these materials were used to fabricate the base material for scaffolds. The base materials were blended at 180 °C, in their molten state, for 5 mins at speed of 60 rpm, using a temperature-controlled mixing chamber (HAAKE RheoDrive 7 & Mixer 600 OS). 3D printing feed-filaments of diameter 3 mm were fabricated using a Noztek single screw filament extruder. Then the filaments were fed into Ultimaker^2 extended+ 3D printer to fabricate lattice structures. Finally, printed lattice

structures were immersed into water to dissolve the sacrificial phases and obtain a hierarchical porous structure in form of lattices, which each bead has intrinsic porosity. In this study, we systematically change blend combinations to optimise mechanical properties. Fig. 1 shows a visual summary of the proposed manufacturing process, from the base materials to the final 3D printed hierarchically porous lattice structure. The details of the procedure, the resulting material microstructures, and their mechanical properties are presented in the following sections.

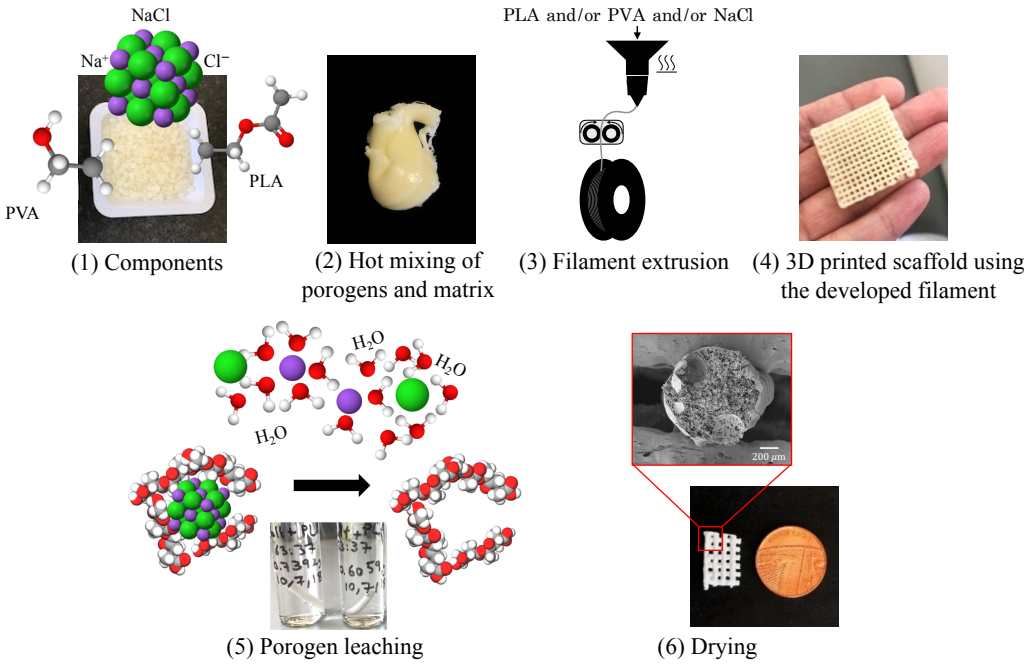

Figure 1: A graphical summary of the proposed manufacturing process —from chemical components to hierarchically porous fabricated lattice: through hot mixing, pelletisation, extrusion, 3D printing, and porogen leaching.

In order to assess the effect of different compositions within blend on the properties of the resulting porous material systematically, the ternary dia-

gram of the material combinations was used; see Fig. 2. Each marker on the graph represents a material combinations prepared in this study. Any point in the middle of the diagram shows the blend of three components, which the concentration of components can be calculated from the corresponding axis. Any point on an extended lines from PLA axis to the apposing apex corresponds to a constant ratio of the PLA to PVA weight fraction. For instance, dashed red line shows all the components with the same PLA to PVA weight ratio of 2.33.

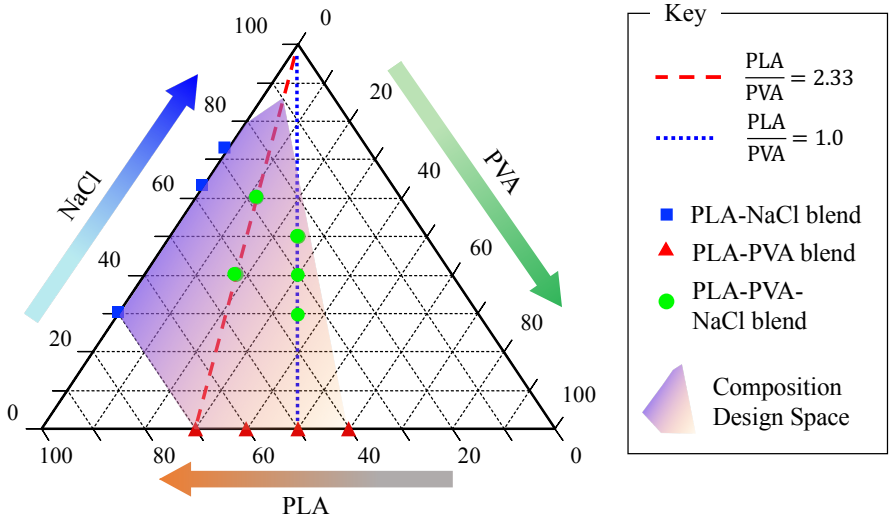

Figure 2: Ternary composition triaxial diagram. Marks on the graph show blend compositions prepared in this study. The blue dotted line shows points on which the PLA to PVA weight ratio is one and the red dashed line represents points on which the PLA to PVA weight ratio is 2.33. The shaded area represents the material combinations explored for optimum manufacturability and mechanical integrity.

2.3. Porosity, connectivity, water uptake

The parameters related to porosity of the scaffold were obtained by gravimetric measurement. Targeted porosity (ϕ) based on theoretical porosity (ϕ_{th}), and connectivity were calculated according to the following expressions [53]:

$$\phi_{\text{th}} = \frac{\left(\frac{m_{\text{NaCl}}}{\rho_{\text{NaCl}}}\right) + \left(\frac{m_{\text{PVA}}}{\rho_{\text{PVA}}}\right)}{\left(\frac{m_{\text{NaCl}}}{\rho_{\text{NaCl}}}\right) + \left(\frac{m_{\text{PVA}}}{\rho_{\text{PVA}}}\right) + \left(\frac{m_{\text{PLA}}}{\rho_{\text{PLA}}}\right)}, \tag{1}$$

$$\phi = \left(1 - \frac{\rho_{\text{scaffold}}}{\rho_{\text{PLA}}}\right), \quad \text{and} \tag{2}$$

$$\text{Connectivity } (\%) = \frac{(m_0 - m_{\text{dry}})}{(m_{\text{NaCl}} + m_{\text{PVA}})} \times 100, \tag{3}$$

where m_{NaCl}, m_{PVA} and m_{PLA} are the theoretical mass of NaCl, PVA and PLA, respectively, assuming homogeneous blends. m_0 is the weight of scaffold before leaching and m_{dry} is the weight of the dried scaffold after porogen leaching. The density (ρ) of PLA, PVA and NaCl are respectively 1.3 g/cm^3, 1.1 g/cm^3 and 2.2 g/cm^3. ρ_{scaffold} is the apparent density of the scaffold. Scanning Electron Microscopy (SEM) is employed to evaluate the pore size and shape in manufactured porous specimens.

2.4. Characterisation

Different material characterisation methods were employed to determine the thermal properties of the blends, porosity level of the produced foams, and their pore size distribution. Thermal properties of the blends are important to be evaluated since they were used in FDM, which includes processing in elevated temperature.

Porogen Weight Loss: In order to assess the effectiveness of the method to create porosity, the rate of porogen dissolution in water was determined by measuring the weight loss of samples after immersing them in water for different time spans. Samples of diameter 5 mm were cut into cylinders of length 15 mm to 25 mm. They were immersed in de-ionized water and were kept in the oven at 50 °C until saturation. After 1, 2, 3, 5, and 9 days the samples were taken out and were kept in the oven at 50 °C for 48 hours, then the dried samples were weighed.

Differential Scanning Calorimetry: Differential Scanning Calorimetry (DSC) is a technique to obtain thermal properties of polymers. The DSC set-up consists of a measurement chamber with two pans that are exposed to controlled heat. The first pan contains the material being characterised and the second one, which is typically empty, is used as a reference. A computer is used to monitor the temperature and to regulate the rate at which the temperature of the pans changes. A typical heating rate is around 10 °C/min.

Mercury Intrusion Porosimetry:

Porosity of the manufactured scaffolds was assessed by mercury intrusion porosimetry technique. The porosity of a material affects its physical properties and, subsequently, its mechanical behaviour. Hence, parameters related to porosity such as pore size, pore volume, pore distribution, and density were determined.

Mechanical Testing: In order to evaluate the mechanical stiffness and strength of the fabricated porous materials, Tinius Olsen H5KS Benchtop

tester was employed to perform uniaxial compression tests. Ten cylindrical samples of each type were prepared and tested according to ASTM D695 standard. The length of samples were approximately 7 mm and their diameter around 4 mm. Considering similar microstructure, these samples are representative of beads in 3D printed lattices. The strain rate for all the tests is set to $2 \times 10^{-3} s^{-1}$. Specific modulus and specific strength were calculated in order to evaluate the effect of porosity level on the mechanical properties of the fabricated porous materials. The underlying deformation mechanisms were then explained using cellular solid theoretical models [36; 37].

3. Results and Discussions

3.1. Porogen Weight Loss:

Results for the porosity and pore interconnectivity of specimens obtained from material combinations are presented in table 2. It can be observed that the more the amount of PVA in the sample, the more is the measured weight loss. In samples with 30% of PVA, the weight loss is around 26% and increasing the weight percentage of PVA causes a weight loss closer to the nominal weight percentage of PVA in the original blend. In other words, when there is more PVA in the blend, it would be easier for all of the PVA to escape from the structure. Small percentages of PVA, by contrast, can be trapped and completely surrounded by PLA, which makes it difficult for them to be removed from the structure by leaching. The load of PVA in the blend is varied in order to prepare samples with different porosities. The resulting porous sample obtained from blends with more than 50% PVA loading did not have adequate mechanical integrity. In these samples, PLA skeleton that

Table 2: Theoretical porosity, measured porosity, connectivity, and PLA/PVA ratio for different blend compositions

Material Combination	ϕ_{th} (%)	ϕ (%)	Connectivity (%)	V_{PLA}/V_{PVA}
PLA:PVA (70%-30%)	33.62	26.1±2.2	94.7±0.1	2.33
PLA:PVA (60%-40%)	44.07	38.2±1.8	95.5±0.1	1.5
PLA:PVA (50%-50%)	54.17	48.0±1.0	98.6±0.1	1
PLA:PVA (40%-60%)	64.50	-	-	0.67
PLA:NaCl (70%-30%)	20.21	20.2±3.2	85.3±0.3	NA
PLA:NaCl (37%-63%)	50.15	45.1 ±2.1	91.8±0.2	NA
PLA:NaCl (30%-70%)	57.96	55.4 ±1.5	92.0±0.3	NA
PLA:PVA:NaCl (42%-18%-40%)	51.67	50.5 ±3.7	97.1±0.5	2.33
PLA:PVA:NaCl (28%-12%-60%)	63.93	66.4±2.4	99.4±0.1	2.33
PLA:PVA:NaCl (25%-25%-50%)	70.27	70.4±1.6	99.5±0.1	1

remained after leaching was found to be too fragile. Hence, in these samples, sedimented PLA was seen after a few days of immersion in water. This is an important finding because it shows that for PLA-PVA blend, there is a balance between porosity and physical integrity and therefore there is a limitation in adding PVA to the blend. This limits the intrinsic porosity level to be approximately 50%.

In specimens with NaCl as porogen, decreasing the amount of NaCl decreases the rate of leaching out from the structure. In these samples, some salt particles is remained in the structure as they are completely trapped by PLA. When the amount of the NaCl in the blend decreases, it takes longer for NaCl to be completely leached out. This was monitored by immersing a PLA:NaCl 70%-30% sample in water for 9 days and then imaging the cross section using SEM. Fig. 3 is a back-scattered SEM image of the cross-section

of the sample and shows that NaCl on the outer layer (as thick as about 1 mm) has dissolved, while it still exists at the centre of the sample. When less NaCl in the blend, particulate leaching occurs relatively slowly. It is challenging to remove all the NaCl from PLA-NaCl blends, because some of the NaCl particles become coated by PLA during the blending process and water cannot diffuse into the structure and dissolve all the NaCl particles. Hence, it is proposed to prepare blends of PLA-PVA-NaCl for 3D printing of bio-constructs. In this approach, different volume percentage of PLA, PVA, and NaCl are blended.

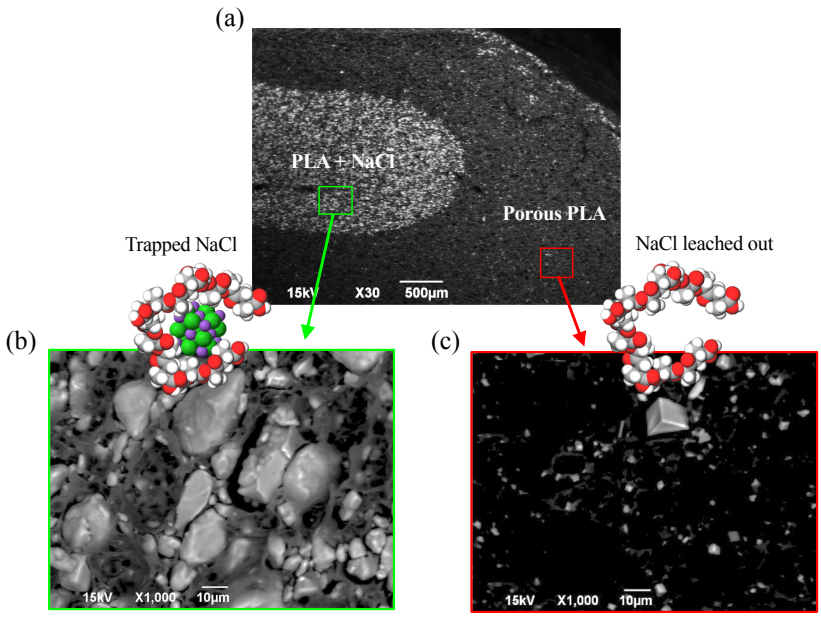

Figure 3: Micrograph of a PLA-NaCl blend specimens after immersing for 9 days in water, (a) back-scattered SEM image of the cross-section, (b) back-scattered image of the middle part, which contains NaCl particles, and (c) back-scattered image of outer section, from where most of the NaCl particles are leached out and a porous structure remains.

3.2. Microstructure, porosity, pore shape and interconnectivity

After complete removal of porogens from the structure of the material, SEM was used to obtain the micrograph of the porous structure. Fig. 4 shows high magnification images of the cross-sections of filaments made of the blends with three different weight percentages of PVA loading. Size and shape of pores are highly dependent on the PLA to PVA ratio. In samples obtained from blends with 30% and 40% PVA weight percentage, the pores are mostly round shaped. In samples with 50% removed PVA, the pores are large and highly interconnected; see Fig. 4c. It is clear that when the percentage of PVA in the blend increases, the pores size increases and subsequently the connectivity within the structure increases, which is beneficial to tissue engineering, however mechanical properties compromises and need to be assessed.

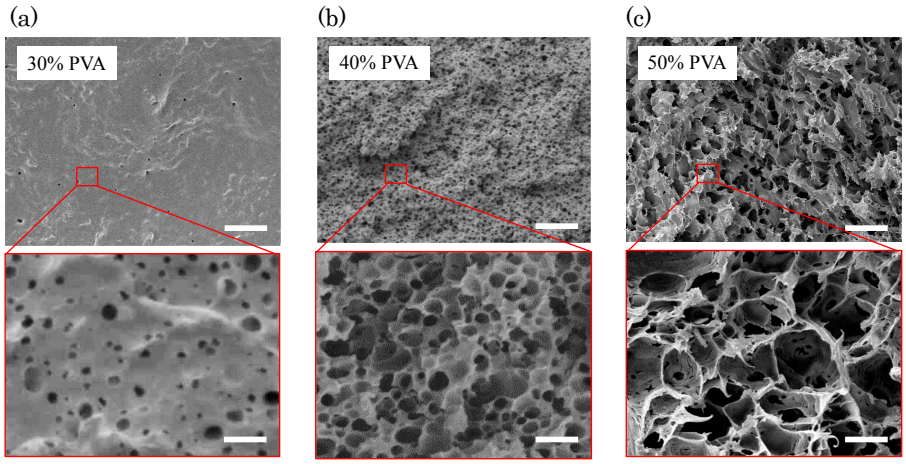

Figure 4: Change in the microstructure obtained from variations in PVA loading from 30% to 50%. Scale bar for the top row figures are 100μm and for the bottom row is 5 μm.

The differential intrusion for porous samples obtained from PLA-PVA

blends are compared in Fig. 5a. The results clearly illustrate how the pore size changes in samples. For PLA:PVA 70%-30% samples as well as PLA:PVA 60%-40% samples, the average size of interconnected pores is in the range of 0.8 μm to 1.2 μm. For PLA:PVA 50%-50% samples, there are two distinguished peaks in the graph, which shows that pores in these samples have a bimodal distribution. One set of pores are centred around 2 μm to 3 μm and another around 7 μm to 8 μm. For PLA:PVA 40%-60% samples, there is only one peak in the graph, which shows the interconnected pores are centred around 30 μm (this has been done on a few sample which survived the leach out step). Fig. 5b shows the pore size distribution in specimens obtained from PLA-NaCl blends. For PLA:NaCl 70%-30% samples, the average size of interconnected pores is in the range of 0.2 μm. In addition, the size of interconnected pores are found to be 1 μm and 8 μm, in PLA:NaCl 37%-63% samples and PLA:NaCl 30%-70% samples, respectively. The difference between the pore size and NaCl particle size, is another indicator of the trapped NaCl particle in the blends.

In specimens obtained from PLA-PVA-NaCl blends, the pore size distribution is compared in Fig. 5c, as quantified by the differential intrusion. For PLA:PVA:NaCl 25%-25%-50% samples, the average size of interconnected pores is in the range of 10 μm. For PLA:PVA:NaCl 42%-18%-40% samples, the size of interconnected pores are around 0.3 μm and for PLA:PVA:NaCl 28%-12%-60% samples, the size of interconnected pores are around 1 μm. The higher intensity of pore size diameters show that PVA can be effective in helping NaCl particles to be washed out more easily. Increasing PVA volume percentage facilitates removal of NaCl from the blend. Microstructure

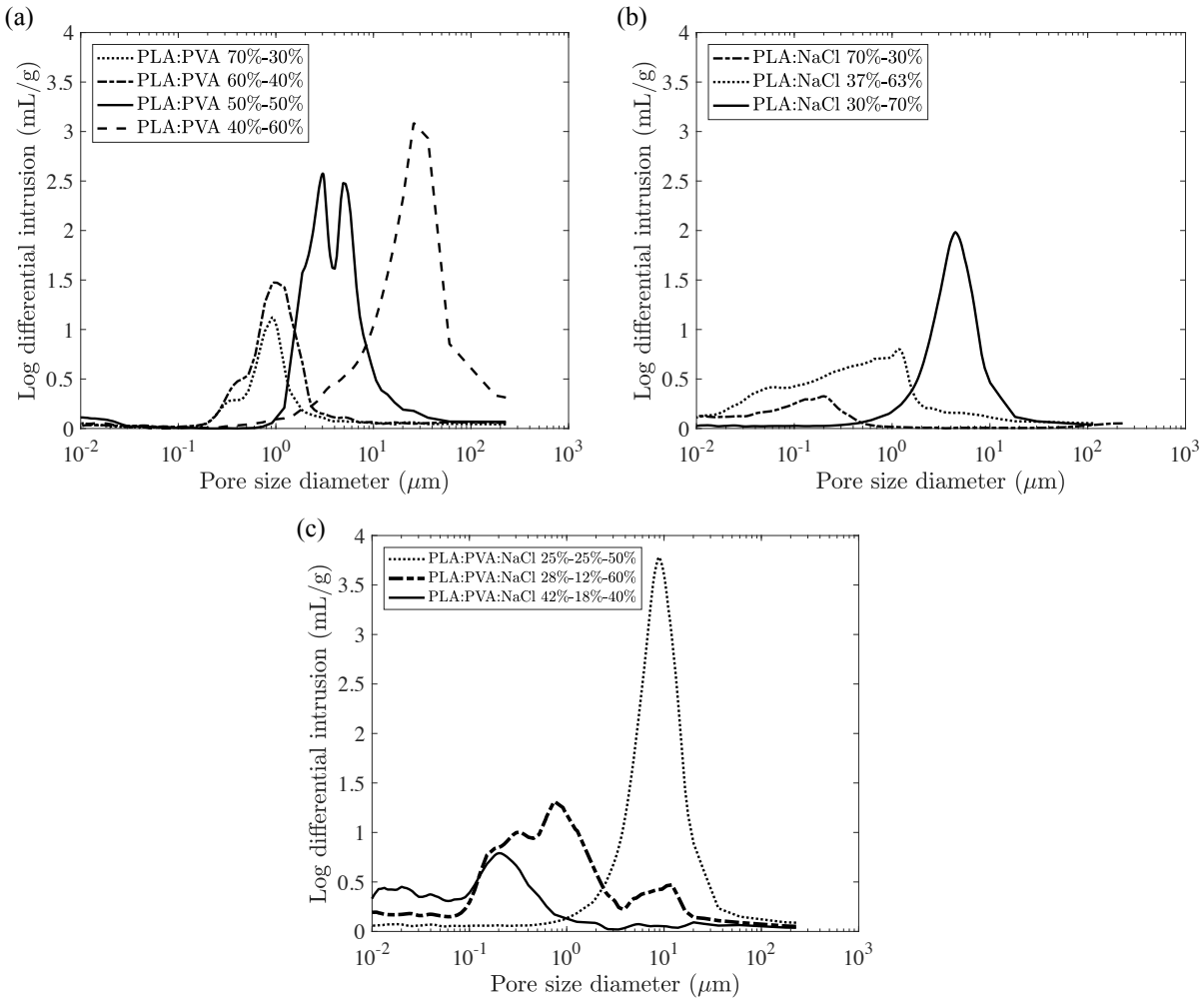

Figure 5: Pore size distribution from mercury intrusion porosimetry for porous PLA obtained from (a) PLA-PVA, (b) PLA-NACl, and (c) PLA-PVA-NaCl blends

of porous materials obtained from PLA-PVA-NaCl blends are shown in SEM images presented in Fig. 6. It is clear that how different blends can lead to different porosity size, shape and distributions. When the ratio of PLA to PVA is higher, i.e. when the amount of PVA is less in the blend, the pores originating from large salt particles ($\sim$100 μm) are clearly visible. Greater amount of PVA in the three-phase blends leads to more interconnected porosity.

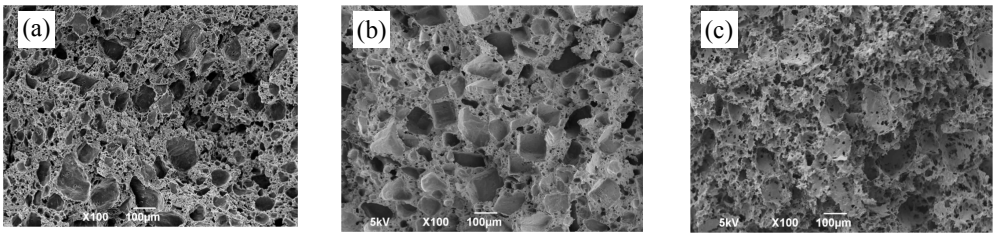

Figure 6: SEM images of the porous samples with different material blends. (a) PLA:PVA:NaCl (42%-18%-40%) 50% of porogen by volume, (b) PLA:PVA:NaCl (28%-12%-60%) 63% of porogen by volume, and (c) PLA:PVA:NaCl (25%-25%-50%) 68% porogen by volume. Weight loss due to leaching of porogens increases from (a) to (c).

3.3. Thermal properties of the polymer and/or NaCl blends

In order to evaluate the thermal properties of the blends, DSC analysis was performed. Thermograms obtained and the associated experimental procedure are presented in appendix. Thermal properties of the blends are key to successful use of these materials in FDM 3D printing. There have been attempts, analogous to colligative properties of solutions, to express the melting temperature of polymer blends as a function of the blend composition. The phase behaviour of polymer blends, by contrast, is rather complex. For

example, the glass transition temperature of blends are often adequately described by the well known Fox's equation [54], given by harmonic mean of the reciprocal of T_g of the components, weighted by the composition. PLA-PVA blends been studied previously by Shuai et al. [55]. Fig. 7 summarizes the effect of PVA percentage on thermal properties of polymer (and NaCl) blends. Increasing PVA volume percentage slightly decreases crystallization (T_c), glass transition (T_g), as well as melting temperature (T_m) of the blends due to its lower glass transition and melting temperature compared to PLA.

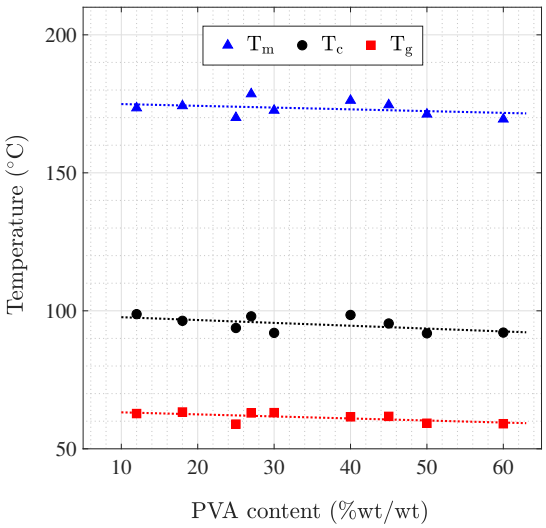

Figure 7: Effect of PVA percentage on thermal properties of polymer (and/or NaCl) blends. Increasing PVA volume percentage decreases crystallization, glass transition, as well as melting temperature of the blends slightly.

3.4. 3D printing with materials containing embedded porogens

The 3D printer feeding filaments fabricated from the two-phase and three-phase blends were used to 3D print square lattice structures. The specimens were then immersed in water for 72 hours followed by a drying step at 50 °C for 48 hours. Fig. 8a shows schematic of the hierarchical structure in which each bead has porous microstructure. The cross section of a typical bead with 50% intrinsic porosity is shown in 8b. An additional extrinsic porosity of the square lattice structure is achieved by spacing between beads. The micrograph of one of the 3D printed lattices is presented in Fig. 8c.

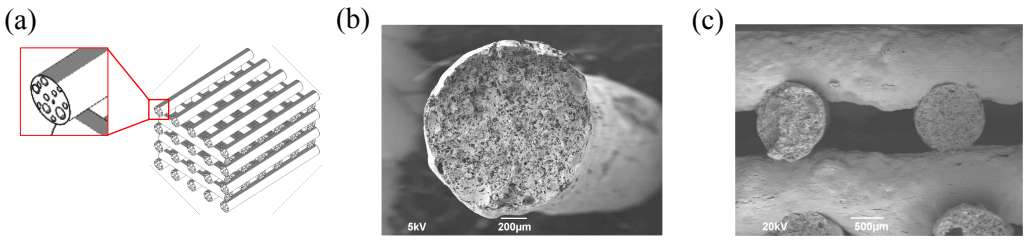

Figure 8: (a) Schematic of a square lattice structure showing *multi-scale porosity* within the struts, unlike usual 3D printed lattice structures that do not show foam within struts, (b) SEM micrograh of an extruded filaments with porous microstructure, and (c) hierarchical porosity within a 3D printed lattice structure, showing relatively large gaps due to spacing of the struts, in addition to smaller scale random pores.

3.5. Mechanical integrity of the porous PLA

Compression test results on porous PLA samples obtained from PLA-PVA blends of 70%-30%, 60%-40%, and 50%-50% are shown in Fig. 9a. As mentioned earlier, samples with 60% PVA could not be tested due to lack of structural integrity. The results show that increasing the volume fraction of

PVA, and subsequently increasing the porosity in the final product, decreases the compressive modulus and strength, and increases the strain at failure. The failure in these samples is usually a brittle failure or involves a strain softening stage.

The results of the compression tests performed on the porous PLA samples obtained from PLA-NaCl blends of 30%-70%, 37%-63% and 70%-30% are shown in Fig. 9b. Increasing the volume fraction of NaCl and subsequently increasing the porosity in the final product, decreases the compressive modulus and strength, and increases the strain at failure. The stress-strain behaviour of these samples demonstrate a strain hardening. These samples do not break, although they show significant barrelling and crushing towards the later stages of deformation. High strength and failure strain can be attributed to the remaining salt particles in their structure.

The compression test results on the porous PLA specimens from three-phase blends are shown in Fig. 9c. Samples obtained from PLA:PVA 50%-50% blend, PLA:NaCl 37%-63% blend, and PLA:PVA:NaCl 42%-18%-40% blend contain 45% to 50% porosity. The average stress vs strain response of samples with fixed porosity level, while formed from different polymer-NaCl blends, is shown in Fig. 9d. These results clearly show that the samples obtained from PLA-NaCl blends possess higher stiffness and strength. However, there are two main problems with these samples: (1) NaCl does not easily leach out from samples with low porosity levels and the remaining NaCl in the structure of biomedical scaffolds is problematic, (2) blends with high amount of NaCl (more than 70%) are not easily printable. At the cost of compromising stiffness and strength, using both PVA and NaCl as poro-

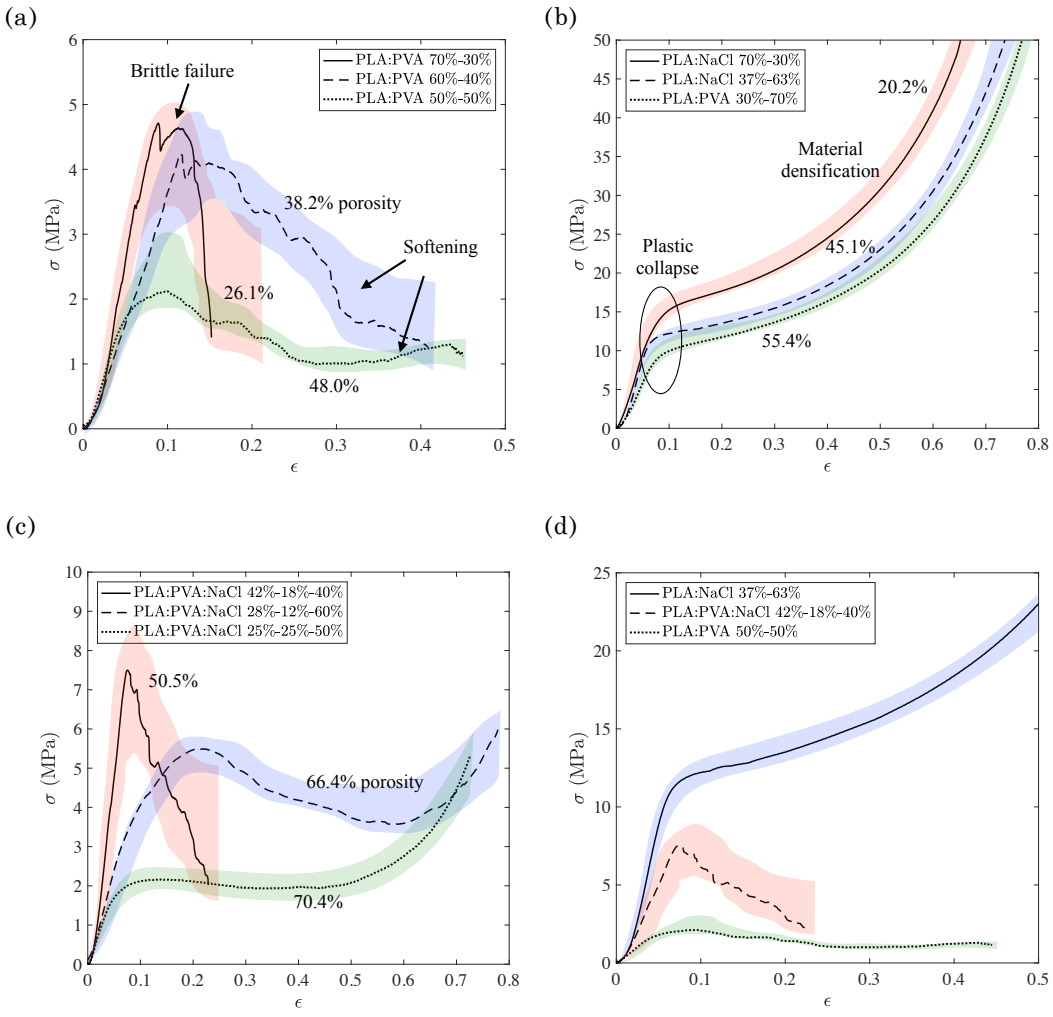

Figure 9: Mean compressive stress-strain curve for porous PLA obtained from (a) PLA-PVA blends, (b) PLA-NaCl blends, (c) PLA-PVA-NaCl blends, and (d) different blends with approximately 50% porosity. The standard deviation is shown using the shaded area.

gens would resolve these issues. Mechanical properties of all specimens are summarized in table 3.

The experimental results show that increasing porogen percentage affects the modulus and strength dramatically. This gives us the possibility of designing materials for a range of applications that demand a range of mechanical properties, in addition to requirements in pore size and the level of porosity. Fig. 10 shows how the compressive modulus of material changes with porosity. Increasing porosity or decreasing the apparent density of material, decreases their elastic modulus for a fixed mesoscopic geometry. To relate the mechanical response of different manufactured porous samples, simple scaling laws for cellular solid models [36; 37] are explored here. The properties of foam structures generally depends on: (1) the material from which the cell walls are made, (2) the relative density of the foam, (3) the degree to which the cells are open or closed, and (4) the shape of the pores. To estimate the apparent elastic modulus of samples, the initial linear part of the stress-strain response was used. For open-cell foams, the elastic modulus of the porous material is given by the following power law [37]:

$$\frac{E}{E_{\mathrm{s}}} = C_1 \left(\frac{\rho}{\rho_{\mathrm{s}}} \right)^2, \tag{4}$$

where E_{s} and ρ_{s} are the elastic modulus and density of the parent solid material and C_1 depends on the parameters such as shape of pores and complexity of the microstructure. The underlying physics behind this power law is that open-cell foams have apparent density scale with the cross-sectional area, whereas the stiffness scales as the second moment of the cross-sectional area, leading to a square dependence of the apparent modulus on the volume

Table 3: Mechanical properties of porous samples obtained from different material blend

Material combination	ρ (g/cm^3)	E (MPa)	σ_{cr} (MPa)	Specific E (kNm/kg)	Specific σ_{cr} (kNm/kg)	Failure mechanism
PLA:PVA (70%-30%)	0.96±0.03	65.2±10.2	4.2±1.1	67.9±10.6	4.4±1.1	Brittle
PLA:PVA (60%-40%)	0.80±0.02	42.3±5.8	3.8±1.3	52.7±7.1	4.7±1.6	Softening
PLA:PVA (50%-50%)	0.67±0.01	29.8±4.9	2.4±0.6	44.1±7.3	3.6±0.9	Softening
PLA:NaCl (70%-30%)	1.03±0.04	172.5±18.6	16.5±2.1	166.3±17.9	15.9±2.1	Plastic collapse
PLA:NaCl (37%-63%)	0.71±0.03	98.2±11.3	10.2±2.4	137.6±15.8	14.3±3.4	Plastic collapse
PLA:NaCl (30%-70%)	0.58±0.02	82.7±9.4	9.0±2.4	142.6±16.2	15.5±4.1	Plastic collapse
PLA:PVA:NaCl (42%-18%-40%)	0.64±0.05	80.4±9.8	7.2±2.1	124.9±15.2	11.2±3.3	Softening
PLA:PVA:NaCl (28%-12%-60%)	0.44±0.03	38.5±8.3	5.0±0.7	88.1±19.0	11.4±1.6	Softening
PLA:PVA:NaCl (25%-25%-50%)	0.38±0.02	25.3±5.7	2.1±0.2	65.7±14.8	5.5±0.5	Plastic collapse

fraction. For closed-cell foams, the relationship is more complicated, which accounts for cell-edge bending and face stretching, and can be written as [36; 37]:

$$\frac{E}{E_{\mathrm{s}}} = C_2 \left(\frac{\rho}{\rho_{\mathrm{s}}}\right)^2 + C_3 \left(\frac{\rho}{\rho_{\mathrm{s}}}\right) \tag{5}$$

where C_2 and C_3 are constant depending on the geometry of the cells. Considering the summarised data presented in Fig. 10a, it can be concluded that the foams obtained from the PLA-NaCl blends have more closed-cell dominant architecture due to the involvement of the linear relationship of relative elastic modulus to the relative density (second term of the equation) and making the slope of the curve less than two. This is consistent with the observations of highly time consuming porogen leaching in PLA-NaCl blends. By contrast, the other blends demonstrate open-cell behaviour, dominated by cell wall bending, as their relative elastic modulus versus relative density has a slope approximately equal to two on a log-log plot. The measured Young's modulus of foams obtained from PLA-PVA blend and PLA-PVA-NaCl blend indicate that the data fit Eq. 4 well, with the constants C_1= 0.09 and 0.03, respectively. Data for Young's modulus of specimens obtained from PLA-NaCl blends, are adequately explained by Eq. 5 with C_2= 0.03 and C_3= 0.04.

There are three different failure mechanisms that are usually observed in the manufactured foams: (1) brittle crushing or brittle collapse, which is observed in samples obtained from PLA-PVA blends, (2) plastic collapse followed by plastic plateau or strain hardening and then material densification, which is mostly observed in samples obtained from PLA-NaCl blends, (3)

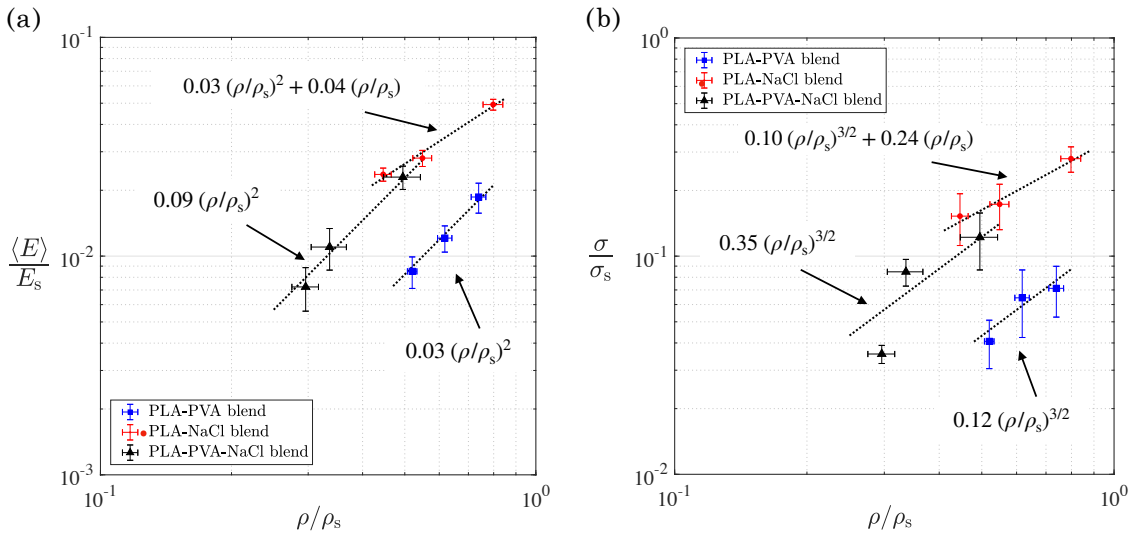

Figure 10: The effect of relative density on (a) normalised elastic modulus and (b) normalised strength of porous material blends. The modulus and the yield strength of the parent material are chosen for normalisation.

plastic collapse followed by a strain softening (and then possible densification in some samples), which is a combination of the first two mechanisms and can be observed in samples obtained from PLA-PVA-NaCl blends. Brittle collapse (crushing) stress is related to the relative density with the following power law expression for open-cell structures [36; 37]:

$$\frac{\sigma_{\text{cr}}}{\sigma_{\text{fs}}} = C_4 \left(\frac{\rho}{\rho_s} \right)^{\frac{3}{2}}, \tag{6}$$

where σ_{fs} is the flextural strength of the parent material and C_4 is a constant. When one accounts for density correction, the above power law becomes a more involved relationship, without a single exponent, and with two terms. If one forced to fit a power law for the strength of such foams through such a functional dependence, one may get an effective exponent between 1.5

and 2 [56]. The strength of samples obtained from PLA-PVA blends agree well with this power law trend. In this failure mechanism, the strength of samples with the same relative density depends on their cell size. The crushing strength decreases with increasing cell size. This phenomenon is observed in comparing PLA:PVA 50%-50% and PLA:PVA:NaCl 42%-18%-40% samples, which have the same relative density but different pore size distribution; see Fig. 5.

In samples obtained from PLA-NaCl blends, the plastic collapse stress relates well with relative density as per the following equation, which is valid for closed-cell dominant structures [36; 37]

$$\frac{\sigma_{\mathrm{pl}}}{\sigma_{\mathrm{y}}} = C_5 \left(\frac{\rho}{\rho_{\mathrm{s}}}\right)^{\frac{3}{2}} + C_6 \left(\frac{\rho}{\rho_{\mathrm{s}}}\right), \tag{7}$$

where σ_{y} is the yield strength of the parent material and C_5 and C_6 are constants. The different slope of data obtained from PLA-NaCl samples is clear in Fig. 10b. Data for strength of specimens obtained from PLA-PVA blend and PLA-PVA-NaCl blend, agrees well with Eq. 6 taking C_4= 0.12 and 0.35, respectively. Measurement of the plastic collapse strength of foams obtained from PLA-NaCl blend indicate that the data are well fitted by Eq. 7 with C_5= 0.10 and C_6= 0.24. A comparison between properties of porous materials obtained from different blends is presented in Fig. 11. Considering interconnected porosity, strength, and Young's modulus, which all are vital for tissue engineering applications, samples obtained from PLA:PVA:NaCl 42%-18%-40% blend demonstrate the most promising properties.

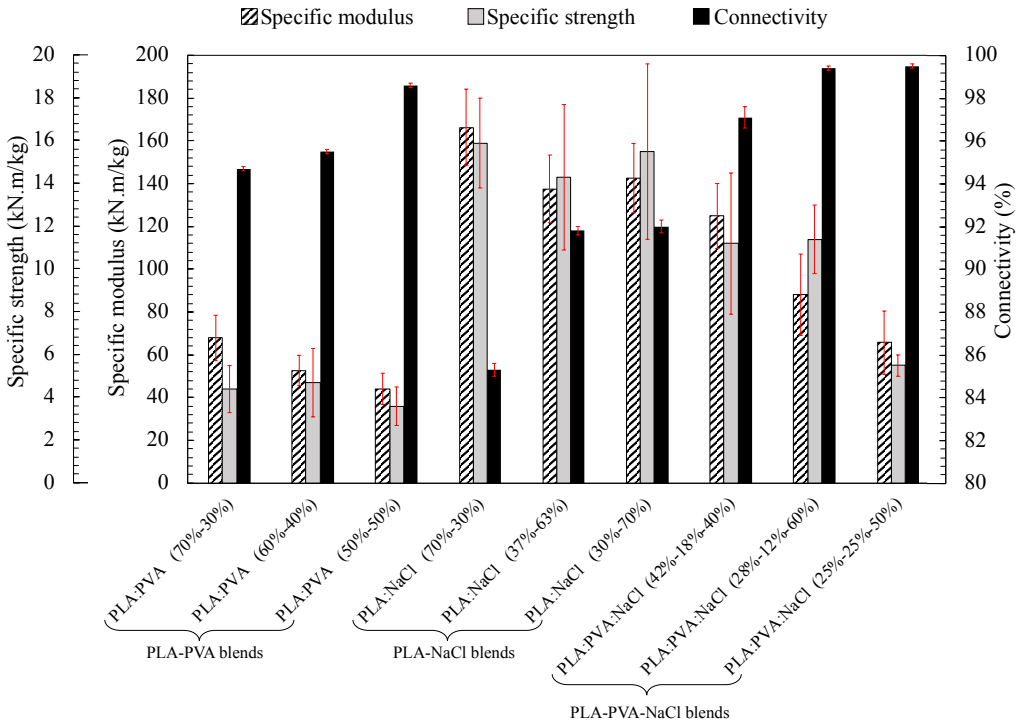

Figure 11: A comparison of the mechanical properties and connectivity of porous samples of different material blends.

4. Conclusions

Advances in additive manufacturing have enabled practical realisation of tissue engineering scaffolds that demonstrate superior mechanical properties, potentially with greater clinical success. Herein, ultra-porous bioresorbable 3D printed PLA scaffolds are fabricated and characterised. PVA and common salt are used as porogens, to introduce intrinsic porosity into the beads within 3D printed lattice structures, which is combined with computer controlled extrinsic porosity. We find that using both PVA and NaCl as porogens overcomes the lack of mechanical integrity found in foams obtained from PLA-PVA blends with the same porosity level and also can improve the manufacturability and pore connectivity of foams obtained from PLA-NaCl blends. For instance, the integrity of filaments obtained from PLA-PVA blends diminishes at 63% porosity (PLA-PVA 40%-60%) levels, while the strength of foams with the same porosity level obtained from PLA-PVA-NaCl blends (PLA:PVA:NaCl 42%-18%-40%) is approximately 7 MPa. Scaffolds with 80% porosity and mechanical integrity are 3D printed with the proposed method. Porogen combination alternates the architecture of pores in the produced foams, which affect the underlying deformation mechanism and correlation between microstructure and mechanical properties. Pore size distribution is assessed using mercury intrusion porosimetry, which relates well with the structures observed in SEM imaging. Evidence of multi-scale porous architecture: random and of tens to hundreds of micron, combined with regular pores at the length scale of a fraction of a millimeter as obtained by computer controlled fabrication, is present in the SEM micrographs. Thermal characterisation of the blends for systematically changing

weight percents of the constituent phases was also carried out.

Theoretical cellular solid models that make use of property vs volume fraction scaling, based on the mechanics of cell wall bending and stretch, as the case may be, are used to estimate appropriate power law trends. Both apparent modulus of elasticity as well as strength are fitted; the exponents seen as consistent with physical expectation. The specimens obtained from the three-phase blends demonstrate properties dominated by open-cell pores. In these specimens, the normalised compressive modulus is proportional to the normalized relative density with power law with exponent two and their normalized compressive strength is proportional to normalized relative density according to a power law with exponent 3/2.

Acknowledgements

Faezeh Shalchy was supported by an EU funded Marie-Curie doctoral training network (HyMedPoly).

References

[1] T. Billiet, M. Vandenhaute, J. Schelfhout, S. Van Vlierberghe, and P. Dubruel, "A review of trends and limitations in hydrogel-rapid prototyping for tissue engineering," *Biomaterials*, vol. 33, pp. 6020–6041, sep 2012.

[2] R. Scaffaro, F. Lopresti, L. Botta, S. Rigogliuso, and G. Ghersi, "Preparation of three-layered porous PLA/PEG scaffold: relationship between morphology, mechanical behavior and cell permeability," *Journal of the Mechanical Behavior of Biomedical Materials*, vol. 54, pp. 8–20, feb 2016.

[3] D. Algul, H. Sipahi, A. Aydin, F. Kelleci, S. Ozdatli, and F. G. Yener, "Biocompatibility of biomimetic multilayered alginatechitosan/β-TCP scaffold for osteochondral tissue," *International Journal of Biological Macromolecules*, vol. 79, pp. 363–369, aug 2015.

[4] X. Cui, S. Xu, W. Su, Z. Sun, Z. Yi, X. Ma, G. Chen, X. Chen, B. Guo, and X. Li, "Freezethaw cycles for biocompatible, mechanically robust scaffolds of human hair keratins," *Journal of Biomedical Materials Research Part B: Applied Biomaterials*, vol. 107, pp. 1452–1461, jul 2019.

[5] J. Y. Park, G. Gao, J. Jang, and D.-W. Cho, "3D printed structures for delivery of biomolecules and cells: tissue repair and regeneration," *Journal of Materials Chemistry B*, vol. 4, pp. 7521–7539, nov 2016.

[6] K. Rezwan, Q. Z. Chen, J. J. Blaker, and A. R. Boccaccini, "Biodegrad-

able and bioactive porous polymer/inorganic composite scaffolds for bone tissue engineering," 2006.

[7] J. M. Sobral, S. G. Caridade, R. A. Sousa, J. F. Mano, and R. L. Reis, "Three-dimensional plotted scaffolds with controlled pore size gradients: effect of scaffold geometry on mechanical performance and cell seeding efficiency," *Acta biomaterialia*, vol. 7, no. 3, pp. 1009–1018, 2011.

[8] X. Chen, H. Fan, X. Deng, L. Wu, T. Yi, L. Gu, C. Zhou, Y. Fan, and X. Zhang, "Scaffold structural microenvironmental cues to guide tissue regeneration in bone tissue applications," *Nanomaterials*, vol. 8, no. 11, p. 960, 2018.

[9] F. S. L. Bobbert and A. A. Zadpoor, "Effects of bone substitute architecture and surface properties on cell response, angiogenesis, and structure of new bone," *J. Mater. Chem. B*, vol. 5, no. 31, pp. 6175–6192, 2017.

[10] S. Gong, H. Wang, Q. Sun, S.-T. Xue, and J.-Y. Wang, "Mechanical properties and in vitro biocompatibility of porous zein scaffolds," *Biomaterials*, vol. 27, pp. 3793–3799, jul 2006.

[11] K. A. Gross and L. M. Rodrguez-Lorenzo, "Biodegradable composite scaffolds with an interconnected spherical network for bone tissue engineering," *Biomaterials*, vol. 25, pp. 4955–4962, sep 2004.

[12] B. Otsuki, M. Takemoto, S. Fujibayashi, M. Neo, T. Kokubo, and T. Nakamura, "Pore throat size and connectivity determine bone and tissue ingrowth into porous implants: Three-dimensional micro-CT based

structural analyses of porous bioactive titanium implants," *Biomaterials*, vol. 27, pp. 5892–5900, dec 2006.

[13] M. J. Moore, E. Jabbari, E. L. Ritman, L. Lu, B. L. Currier, A. J. Windebank, and M. J. Yaszemski, "Quantitative analysis of interconnectivity of porous biodegradable scaffolds with micro-computed tomography," *Journal of Biomedical Materials Research*, vol. 71A, pp. 258–267, nov 2004.

[14] Y. Reinwald, R. K. Johal, A. M. Ghaemmaghami, F. R. Rose, S. M. Howdle, and K. M. Shakesheff, "Interconnectivity and permeability of supercritical fluid-foamed scaffolds and the effect of their structural properties on cell distribution," *Polymer (United Kingdom)*, vol. 55, pp. 435–444, jan 2014.

[15] F. J. Hua, G. E. Kim, J. D. Lee, Y. K. Son, and D. S. Lee, "Macroporous poly(L-lactide) scaffold 1. Preparation of a macroporous scaffold by liquid-liquid phase separation of a PLLA-dioxane-water system," *Journal of Biomedical Materials Research*, vol. 63, no. 2, pp. 161–167, 2002.

[16] Y. S. Nam and T. G. Park, "Porous biodegradable polymeric scaffolds prepared by thermally induced phase separation," *Journal of Biomedical Materials Research*, vol. 47, pp. 8–17, oct 1999.

[17] R. C. Thomson, M. J. Yaszemski, J. M. Powers, and A. G. Mikos, "Fabrication of biodegradable polymer scaffolds to engineer trabecular bone.,"

Journal of biomaterials science. Polymer edition, vol. 7, no. 1, pp. 23–38, 1995.

[18] R. C. Thomson, M. J. Yaszemski, J. M. Powers, T. P. Harrigan, and A. G. Mikos, "Poly(α-Hydroxy Ester)/Short Fiber Hydroxyapatite Composite Foams for Orthopedic Application," *MRS Proceedings*, vol. 394, p. 25, jan 1995.

[19] H. Schoof, L. Bruns, A. Fischer, I. Heschel, and G. Rau, "Dendritic ice morphology in unidirectionally solidi"ed collagen suspensions," *Journal of Crystal Growth*, vol. 209, pp. 122–129, 2000.

[20] H. Schoof, J. Rn Apel, I. Heschel, and G. Nter Rau, "Control of Pore Structure and Size in Freeze-Dried Collagen Sponges," *J Biomed Mater Res (Appl Biomater)*, vol. 58, pp. 352–357, 2001.

[21] N. Dagalakis, J. Flink, P. Stasikelis, J. F. Burke, and I. V. Yannas, "Design of an artificial skin. Part III. Control of pore structure," *Journal of Biomedical Materials Research*, vol. 14, pp. 511–528, jul 1980.

[22] C. J. Doillon, C. F. Whyne, S. Brandwein, and F. H. Silver, "Collagen-based wound dressings: Control of the pore structure and morphology," *Journal of Biomedical Materials Research*, vol. 20, pp. 1219–1228, oct 1986.

[23] Reuber, M., L. S. Yu and W. J. Kolff., "Effect of processing temperature on the properties of polyurethane and comparison of vacuum forming and solution casting to make artificial hearts," *Artificial Organs*, vol. 11, 1987.

[24] D. W. Hutmacher, T. Schantz, I. Zein, K. W. Ng, S. H. Teoh, and K. C. Tan, "Mechanical properties and cell cultural response of polycaprolactone scaffolds designed and fabricated via fused deposition modeling," *Journal of Biomedical Materials Research*, vol. 55, pp. 203–216, may 2001.

[25] A. A. Zadpoor, "Mechanical performance of additively manufactured meta-biomaterials," *Acta biomaterialia*, vol. 85, pp. 41–59, 2019.

[26] H. Kolken, K. Lietaert, T. van der Sloten, B. Pouran, A. Meynen, G. Van Loock, H. Weinans, L. Scheys, and A. A. Zadpoor, "Mechanical performance of auxetic meta-biomaterials," *journal of the mechanical behavior of biomedical materials*, vol. 104, p. 103658, 2020.

[27] Z. S. Bagheri, D. Melancon, L. Liu, R. B. Johnston, and D. Pasini, "Compensation strategy to reduce geometry and mechanics mismatches in porous biomaterials built with selective laser melting," *Journal of the mechanical behavior of biomedical materials*, vol. 70, pp. 17–27, 2017.

[28] E. O. Bachtiar, O. Erol, M. Millrod, R. Tao, D. H. Gracias, L. H. Romer, and S. H. Kang, "3d printing and characterization of a soft and biostable elastomer with high flexibility and strength for biomedical applications," *Journal of the Mechanical Behavior of Biomedical Materials*, vol. 104, p. 103649, 2020.

[29] M. M. Porter, N. Ravikumar, F. Barthelat, and R. Martini, "3d-printing and mechanics of bio-inspired articulated and multi-material

structures," *Journal of the mechanical behavior of biomedical materials*, vol. 73, pp. 114–126, 2017.

[30] Y. Zamani, G. Amoabediny, J. Mohammadi, H. Seddiqi, M. N. Helder, B. Zandieh-Doulabi, J. Klein-Nulend, and J. H. Koolstra, "3d-printed poly (-caprolactone) scaffold with gradient mechanical properties according to force distribution in the mandible for mandibular bone tissue engineering," *Journal of the Mechanical Behavior of Biomedical Materials*, p. 103638, 2020.

[31] X. Mu, T. Bertron, C. Dunn, H. Qiao, J. Wu, Z. Zhao, C. Saldana, and H. J. Qi, "Porous polymeric materials by 3D printing of photocurable resin," *Materials Horizons*, vol. 4, pp. 442–449, may 2017.

[32] A. E. Jakus, N. R. Geisendorfer, P. L. Lewis, and R. N. Shah, "3D-printing porosity: A new approach to creating elevated porosity materials and structures," *Acta Biomaterialia*, vol. 72, pp. 94–109, may 2018.

[33] F. Baino, E. Fiume, J. Barberi, S. Kargozar, J. Marchi, J. Massera, and E. Verné, "Processing methods for making porous bioactive glass-based scaffolds—A state-of-the-art review," *International Journal of Applied Ceramic Technology*, vol. 16, no. 5, pp. 1762–1796, 2019.

[34] T. L. Conrad and R. K. Roeder, "Effects of porogen morphology on the architecture, permeability, and mechanical properties of hydroxyapatite whisker reinforced polyetheretherketone scaffolds," *Journal of the Mechanical Behavior of Biomedical Materials*, p. 103730, 2020.

[35] L. Draghi, S. Resta, M. G. Pirozzolo, and M. C. Tanzi, "Microspheres leaching for scaffold porosity control," *Journal of materials science: materials in medicine*, vol. 16, no. 12, pp. 1093–1097, 2005.

[36] L. J. Gibson and M. F. Ashby, *Cellular solids : structure and properties*. Cambridge University Press, 1997.

[37] L. J. Gibson, "Biomechanics of cellular solids," *Journal of Biomechanics*, 2005.

[38] Y. Ramot, M. Haim-Zada, A. J. Domb, and A. Nyska, "Biocompatibility and safety of pla and its copolymers," *Advanced drug delivery reviews*, vol. 107, pp. 153–162, 2016.

[39] J. Chen, B. Chu, and B. S. Hsiao, "Mineralization of hydroxyapatite in electrospun nanofibrous poly(L-lactic acid) scaffolds," *Journal of Biomedical Materials Research Part A*, vol. 79A, pp. 307–317, nov 2006.

[40] X.-L. Deng, G. Sui, M.-L. Zhao, G.-Q. Chen, and X.-P. Yang, "Poly(L-lactic acid)/hydroxyapatite hybrid nanofibrous scaffolds prepared by electrospinning," *Journal of Biomaterials Science, Polymer Edition*, vol. 18, pp. 117–130, jan 2007.

[41] S. I. Jeong, E. K. Ko, J. Yum, C. H. Jung, Y. M. Lee, and H. Shin, "Nanofibrous Poly(lactic acid)/Hydroxyapatite Composite Scaffolds for Guided Tissue Regeneration," *Macromolecular Bioscience*, vol. 8, pp. 328–338, apr 2008.

[42] H.-W. Kim, H.-H. Lee, and J. C. Knowles, "Electrospinning biomedical

nanocomposite fibers of hydroxyapatite/poly(lactic acid) for bone regeneration," *Journal of Biomedical Materials Research Part A*, vol. 79A, pp. 643–649, dec 2006.

[43] M. Peesan, R. Rujiravanit, and P. Supaphol, "Electrospinning of hexanoyl chitosan/polylactide blends," *Journal of Biomaterials Science, Polymer Edition*, vol. 17, pp. 547–565, jan 2006.

[44] P. Sangsanoh, S. Waleetorncheepsawat, O. Suwantong, P. Wutticharoenmongkol, O. Weeranantanapan, B. Chuenjitbuntaworn, P. Cheepsunthorn, P. Pavasant, and P. Supaphol, "In vitro biocompatibility of schwann cells on surfaces of biocompatible polymeric electrospun fibrous and solution-cast film scaffolds," *Biomacromolecules*, vol. 8, no. 5, pp. 1587–1594, 2007.

[45] I. Manavitehrani, A. Fathi, Y. Wang, P. K. Maitz, and F. Dehghani, "Reinforced Poly(Propylene Carbonate) Composite with Enhanced and Tunable Characteristics, an Alternative for Poly(lactic Acid)," *ACS Applied Materials & Interfaces*, vol. 7, pp. 22421–22430, oct 2015.

[46] N. Ashammakhi and P. Rokkanen, "Absorbable polyglycolide devices in trauma and bone surgery," *Biomaterials*, vol. 18, pp. 3–9, jan 1997.

[47] I. Bisson, M. Kosinski, S. Ruault, B. Gupta, J. Hilborn, F. Wurm, and P. Frey, "Acrylic acid grafting and collagen immobilization on poly(ethylene terephthalate) surfaces for adherence and growth of human bladder smooth muscle cells," *Biomaterials*, vol. 23, pp. 3149–3158, aug 2002.

[48] C.-F. Mu, P. Balakrishnan, F.-D. Cui, Y.-M. Yin, Y.-B. Lee, H.-G. Choi, C. S. Yong, S.-J. Chung, C.-K. Shim, and D.-D. Kim, "The effects of mixed MPEGPLA/Pluronic® copolymer micelles on the bioavailability and multidrug resistance of docetaxel," *Biomaterials*, vol. 31, pp. 2371–2379, mar 2010.

[49] Y. Zhang, W. Fan, Z. Ma, C. Wu, W. Fang, G. Liu, and Y. Xiao, "The effects of pore architecture in silk fibroin scaffolds on the growth and differentiation of mesenchymal stem cells expressing BMP7," *Acta Biomaterialia*, vol. 6, pp. 3021–3028, aug 2010.

[50] X. Zheng, B. Kan, M. Gou, S. Fu, J. Zhang, K. Men, L. Chen, F. Luo, Y. Zhao, X. Zhao, Y. Wei, and Z. Qian, "Preparation of MPEGPLA nanoparticle for honokiol delivery in vitro," *International Journal of Pharmaceutics*, vol. 386, pp. 262–267, feb 2010.

[51] K. Yamaura, M. Tada, T. Tanigami, and S. Matsuzawa, "Mechanical properties of films of poly (vinyl alcohol) derived from vinyl trifluoroacetate," *Journal of applied polymer science*, vol. 31, no. 2, pp. 493–500, 1986.

[52] Z. Yanlin, Y. ZHANG, and W. Wen, "Mechanical properties of bedded rock salt and creep failure model," *Mineral Engineering and Research*, vol. 25, no. 1, pp. 16–20, 2010.

[53] R. M. Allaf, I. V. Rivero, N. Abidi, and I. N. Ivanov, "Porous poly(ϵ-caprolactone) scaffolds for load-bearing tissue regeneration: Solventless fabrication and characterization," *Journal of Biomedical Materials Re-*

search - Part B Applied Biomaterials, vol. 101 B, pp. 1050–1060, aug 2013.

[54] T. G. Fox, "Influence of diluent and of copolymer composition on the glass temperature of a polymer system," *Bull. Am. Phys. Soc.*, vol. 1, p. 123, 1956.

[55] X. Shuai, Y. He, N. Asakawa, and Y. Inoue, "Miscibility and phase structure of binary blends of poly (l-lactide) and poly (vinyl alcohol)," *Journal of applied polymer science*, vol. 81, no. 3, pp. 762–772, 2001.

[56] F. C. Oliveira, S. Dias, M. F. Vaz, and J. C. Fernandes, "Behaviour of open-cell cordierite foams under compression," *Journal of the European Ceramic Society*, vol. 26, no. 1-2, pp. 179–186, 2006.

Appendix

Differential Scanning Calorimetry (DSC) is a colorimetric technique used to obtain thermal properties of polymers, for example, the melting point of a crystalline polymer or the glass transition temperature of a non-crystalline polymer. In order to evaluate thermal properties of the blends, a dynamic DSC analysis using METTLER TOLEDO DSC 3^+ apparatus was performed on different material blends in the range of 25-250 °C in order to evaluate the influence of the presence of the NaCl and PVA on the glass transition temperature T_g, crystallization temperature T_c, and melting temperature T_m of the neat PLA. A comparison between the DSC thermograms is reported in Fig. 12. Peaks on these graphs show T_g, T_c, and T_m.

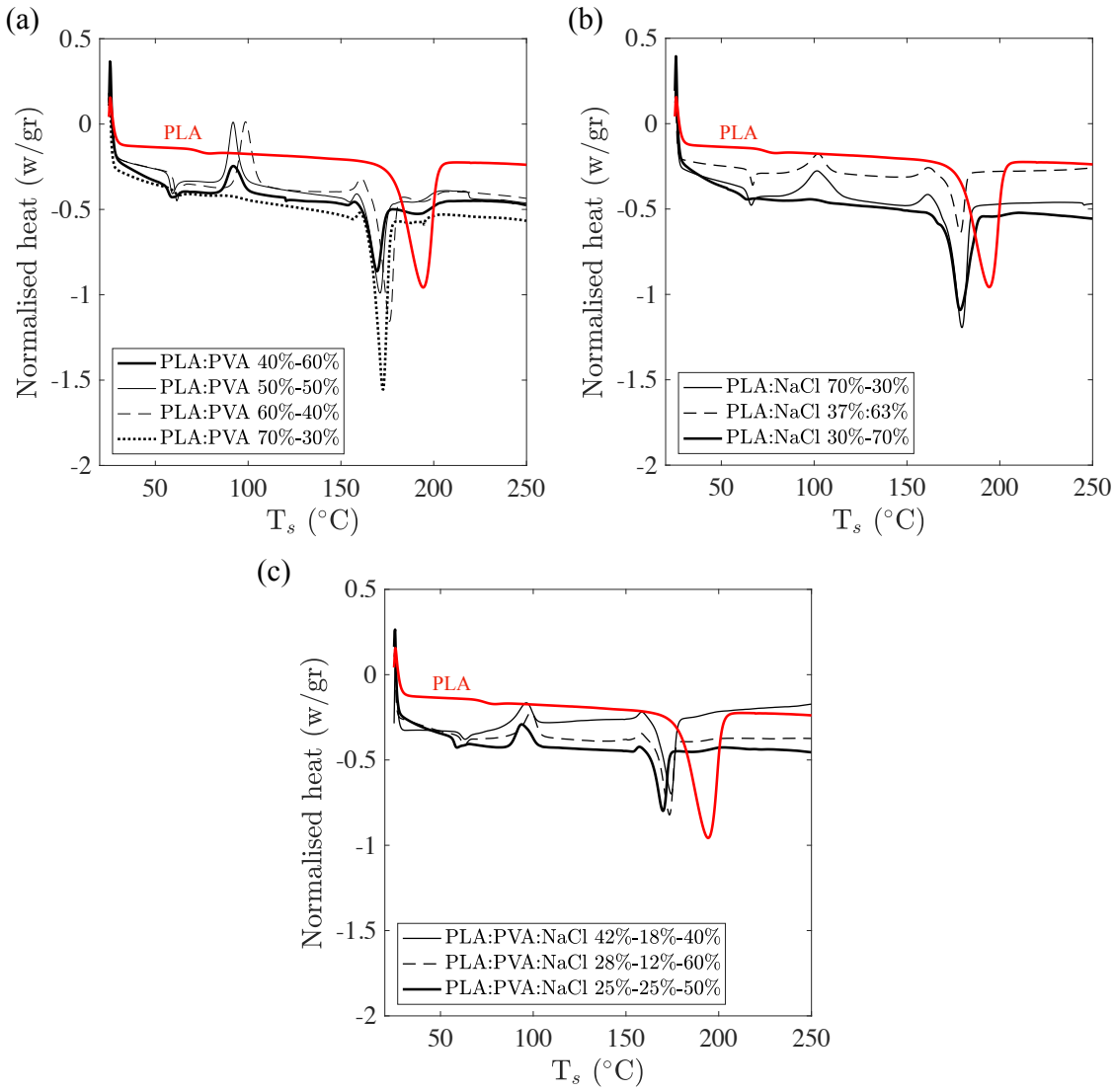

Figure 12: DSC analysis on blends of (a) PLA-PVA, (b) PLA-NaCl, and (c) PLA-PVA-NaCl.